JOURNAL OF GUIDANCE, CONTROL, AND DYNAMICS
Vol. 27, No. 1, January–February 2004

Control of a Nonlinear Wing Section Using Leading- and Trailing-Edge Surfaces

George Platanitis* and Thomas W. Strganac†
Texas A&M University, College Station, Texas 77843-3141

The control of nonlinear aeroelastic response of a wing section with a continuous stiffening-type structural nonlinearity is examined through analytical and experimental studies. Motivated by the limited effectiveness of using a single, trailing-edge control surface for the suppression of limit-cycle oscillations of a typical wing section, improvements in the control of limit-cycle oscillations are investigated through the use of multiple control surfaces, namely, an additional leading-edge control surface. The control methodology consists of a feedback linearization approach that transforms the system equations of motion via Lie algebraic methods and a model reference adaptive control strategy that augments the closed-loop system to account for inexact cancellation of nonlinear terms due to modeling uncertainty. Specifically, uncertainty in the nonlinear pitch stiffness is examined. It is shown through simulations and experiments that globally stabilizing control may be achieved by using two control surfaces.

Nomenclature

a	=	nondimensional distance from midchord to elastic axis position
b	=	semichord of wing section
C_l	=	wing section lift coefficient
$C_{l\alpha}, C_{l\beta}, C_{l\gamma}$	=	$\partial C_l/\partial\alpha, \partial C_l/\partial\beta, \partial C_l/\partial\gamma$
$C_{m-c/4}$	=	wing section moment coefficient at quarter-chord
$C_{m\alpha}, C_{m\beta}, C_{m\gamma}$	=	$\partial C_{m-c/4}/\partial\alpha, \partial C_{m-c/4}/\partial\beta, \partial C_{m-c/4}/\partial\gamma$
c_h	=	plunge damping
c_α	=	pitch damping
h	=	plunge displacement
I_{cam}	=	pitch cam moment of inertia
$I_{\text{cg-wing}}$	=	wing section moment of inertia about the center of gravity
I_α	=	total pitch moment of inertia about elastic axis
k_h	=	plunge stiffness
m_T	=	total mass of pitch–plunge system
m_{wing}	=	mass of wing section
$m_{W-\text{tot}}$	=	total wing section plus mount mass
r_{cg}	=	distance from elastic axis to center of mass
s	=	wing section span
U	=	freestream velocity
x_α	=	nondimensional distance from elastic axis to center of mass
α	=	angle of attack
β	=	trailing-edge control surface deflection
γ	=	leading-edge control surface deflection
ρ	=	air density

Introduction

AEROELASTICITY is the field of study that describes the response and stability characteristics of physical systems due to the interaction of structural, inertial, and aerodynamic forces. As characteristics such as flowfield conditions change, the aeroelastic structure may encounter adverse instabilities such as flutter. Many studies are directed to developing strategies for the suppression of flutter by active control. For example, Rule et al.[1] designed a wing model for studies of flutter control, Wazak and Srinathkumar,[2] as well as Mukhopadhyay,[3] examined control with experimental validation for the active flexible wing, and Vipperman et al.[4] developed a control strategy with experiment validation using μ-synthesis approaches.

In recent years, attention has been given to the presence of limit-cycle oscillations (LCOs), which are attributed to nonlinearities in the aeroelastic system.[5,6] Several control strategies with focus on the control of nonlinear behavior in aeroelastic systems have been examined. In several papers, the authors[7–9] examined various nonlinear control strategies to suppress flutter and nonlinear responses. The control laws developed were applied to a wing section with a single, full-span, trailing-edge control surface and validated in wind-tunnel experiments. Block and Strganac[7] made use of Theodorsen's unsteady aerodynamic model and implemented a linear controller derived via the linear quadratic regulator (LQG) approach combined with a Kalman estimator to provide the additional, nonmeasurable states resulting from Theodorsen's function and servomotor dynamics. The controller stabilized the system if activated during the transient phase of the motion, but its capability was limited once the system was entrained in LCO motion. Ko et al.[8] developed a control law using partial feedback linearization via Lie algebraic methods. The pitch degree of freedom was chosen as the primary variable to control because the system could be transformed to cancel out the nonlinearities introduced by the torsion stiffness. Any conventional linear method could then be applied to control the system. Ko et al.[9] studied the parametric stability and bifurcation structure of the resulting closed-loop dynamics. It was shown that the use of a partial feedback linearization scheme would lead to a locally stable controller. With limitation to a single control surface, it was found that feedback linearization stabilized LCOs to new, multiple, nonzero equilibria that depended on the state at control activation (also see Ref. 8).

The limitations of linear control on the nonlinear system emphasize the necessity for nonlinear control, particularly in the area of adaptive control design, where adaptive methods may be implemented to account for modeling uncertainties, especially those presented by nonlinearities. Progress in adaptive control methodologies provided new, expanded capabilities for control of the aeroelastic system. Xing and Singh[10] designed an adaptive control approach using output feedback based on the assumption that only the pitch angle and plunge displacement were measured, while all other system parameters were unknown. Estimates of the pitch and plunge time derivatives were derived from a canonical state variable

Received 13 January 2002; presented as Paper 2002-1718 at the AIAA 43rd Structures, Structural Dynamics, and Materials Conference, Denver, CO, 22–25 April 2002; revision received 11 June 2003; accepted for publication 12 June 2003.

*Graduate Research Assistant, Department of Aerospace Engineering.
†Associated Professor, Department of Aerospace Engineering. Associate Fellow AIAA.

representation of the system and the use of filters. Zhang and Singh[11] designed an adaptive control model for a system with unstructured model uncertainties.

Because control with feedback linearization requires the exact cancellation of the nonlinear parameters,[8] adaptive methods were introduced to account for uncertainties in the nonlinear parameters.[12–14] When adaptive control methods based on the standard model reference approach were used, LCOs were stabilized to the zero equilibrium point for the wing section with a single trailing-edge control surface. In practice, the freestream velocity at which this adaptive control worked well was approximately 23% greater than the velocity of LCO onset. Further improvement was made to the controller through the development of the structured model reference adaptive controller,[15] which suppressed flutter of the wing section at all velocities within the wind-tunnel range.

Although LCO control has been successful using a single control surface at the trailing edge, the extension of control theory to a wing section with multiple control surfaces is of interest in an attempt to improve performance. Furthermore, with two control surfaces, it is possible to achieve a globally stabilizing controller.[8,9] Herein, the extension and validation of control laws as applied to a wing section with both a leading- and trailing-edge full-span control surface is studied.

System Model

Although our wing system has four degrees of freedom, the high-frequency dynamics of the control surfaces are assumed to be far removed from the dynamics of the primary system. Thus, the equations of motion for a wing section with two degrees of freedom appear in the familiar form

$$\begin{bmatrix} m_T & m_W x_\alpha b \\ m_W x_\alpha b & I_\alpha \end{bmatrix} \begin{Bmatrix} \ddot{h} \\ \ddot{\alpha} \end{Bmatrix} + \begin{bmatrix} c_h & 0 \\ 0 & c_a \end{bmatrix} \begin{Bmatrix} \dot{h} \\ \dot{\alpha} \end{Bmatrix} + \begin{bmatrix} k_h & 0 \\ 0 & k_\alpha \end{bmatrix} \begin{Bmatrix} h \\ \alpha \end{Bmatrix} = \begin{Bmatrix} -L(t) \\ M(t) \end{Bmatrix} \tag{1}$$

where it is noted that the terms in the mass matrix are defined to be consistent with the experimental hardware.

The lift L and moment M are quasi-steady aerodynamic forces and moments, respectively, including both a leading-edge and a trailing-edge control surface, and are defined as

$$L = \rho U^2 bs C_{l_\alpha}\left[\alpha + (\dot{h}/U) + \left(\tfrac{1}{2} - a\right)b(\dot{\alpha}/U)\right] + \rho U^2 bs C_{l_\beta}\beta + \rho U^2 bs C_{l_\gamma}\gamma$$

$$M = \rho U^2 b^2 s C_{m_{\alpha-\text{eff}}}\left[\alpha + (\dot{h}/U) + \left(\tfrac{1}{2} - a\right)b(\dot{\alpha}/U)\right] + \rho U^2 b^2 s C_{m_{\beta-\text{eff}}}\beta + \rho U^2 b^2 s C_{m_{\gamma-\text{eff}}}\gamma \tag{2}$$

where $C_{m_{\alpha-\text{eff}}}$, $C_{m_{\beta-\text{eff}}}$, and $C_{m_{\gamma-\text{eff}}}$ are the effective dynamic and control moment derivatives due to angle of attack and trailing- and leading-edge control surface deflection, respectively, about the elastic axis and are defined as follows:

$$C_{m_{\alpha-\text{eff}}} = \left(\tfrac{1}{2} + a\right)C_{l_\alpha} + 2C_{m_\alpha}, \qquad C_{m_{\beta-\text{eff}}} = \left(\tfrac{1}{2} + a\right)C_{l_\beta} + 2C_{m_\beta}$$

$$C_{m_{\gamma-\text{eff}}} = \left(\tfrac{1}{2} + a\right)C_{l_\gamma} + 2C_{m_\gamma} \tag{3}$$

Recall that $C_{m_\alpha} = 0$ for a symmetric airfoil. This model has proven to be adequate for low reduced frequency, subsonic flow, as validated by the experiments.[7,8,15]

The wing section modeled by these equations of motion has been built for experiments on the nonlinear aeroelastic test apparatus (NATA)[16] in the 2×3 ft low-speed wind tunnel. A unique feature of NATA is the presence of two cams that are fabricated to permit prescribed nonlinear responses in pitch and plunge. The parameters of the experiment and in Eqs. (1) and (2) are given in Table 1. The NATA testbed has been used successfully for investigations in the linear and nonlinear response of wing sections in addition to the development of control methods. Figures 1 and 2 show the apparatus. Two FUTABA S9402 servomotors actuate the control surfaces, each motor being capable of generating $0.654\ \text{N} \cdot \text{m}$ of torque at 5 V, with deflections of the control surfaces linearly proportional to the applied voltage. In addition, two E2-1024-375-H optical encoders are mounted on the rotation shafts of the leading- and trailing-edge control surfaces to allow measurement of the control surface deflections so that they can be compared to the commanded inputs. The sizes of the leading- and trailing-edge control surfaces are 15 and 20% chord length, respectively. Figure 3 is a photograph showing the wing section model.

Table 1 System parameters

Parameter	Value
ρ	$1.225\ \text{kg/m}^3$
a	-0.6719
b	0.1905 m
r_{cg}	$-b(0.0998 + a)$
x_α	r_{cg}/b
s	0.5945 m
k_h	2844 N/m
c_h	27.43 kg/s
c_α	$0.0360\ \text{kg} \cdot \text{m}^2/\text{s}$
m_{wing}	4.340 kg
$m_{W-\text{tot}}$	5.230 kg
m_T	15.57 kg
I_{cam}	$0.04697\ \text{kg} \cdot \text{m}^2$
$I_{\text{cg-wing}}$	$0.04342\ \text{kg} \cdot \text{m}^2$
I_α	$I_{\text{cam}} + I_{\text{cg-wing}} + m_{\text{wing}} r_{\text{cg}}^2$
C_{l_α}	6.757
C_{l_β}	3.774
C_{m_β}	-0.6719
C_{l_γ}	-0.1566
C_{m_γ}	-0.1005

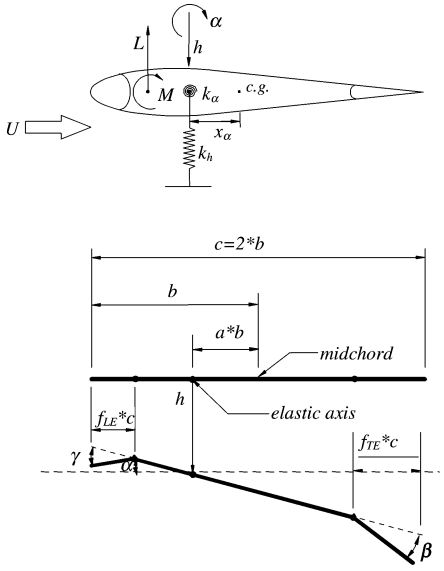

Fig. 1 Aeroelastic system with two-degree-of-freedom motion; new airfoil design has both a leading- and trailing-edge control surface for suppressing flutter and limit-cycle motion.

Feedback Linearization, Leading- and Trailing-Edge Control Configuration

In Ref. 8, Ko et al. develop the full-feedback linearization model on which we build for the two control surface control model. Because feedback linearization serves as a basis on which adaptive control methods will be used to augment control, we repeat the following equations with description as essential for the work herein, with an emphasis on the leading-edge–trailing-edge control surface configuration. Equations (1) and (2) are combined to form the following

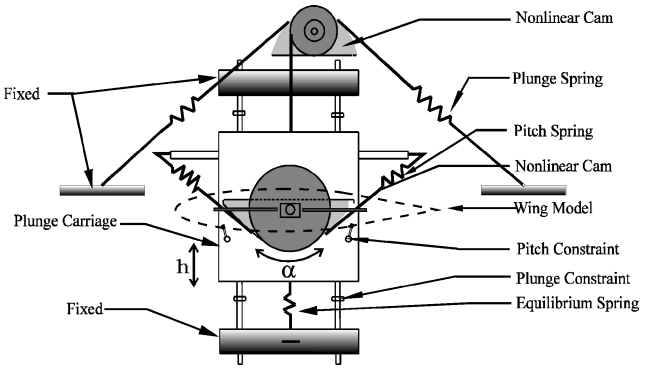

Fig. 2 NATA model support system that permits prescribed nonlinear motion in two degrees of freedom.

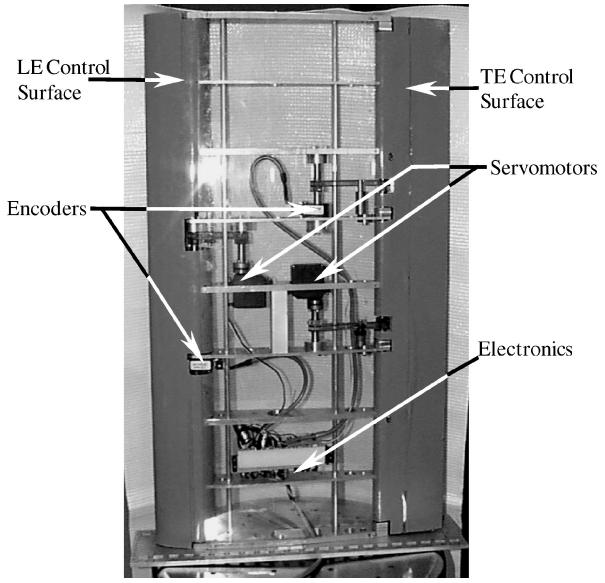

a)

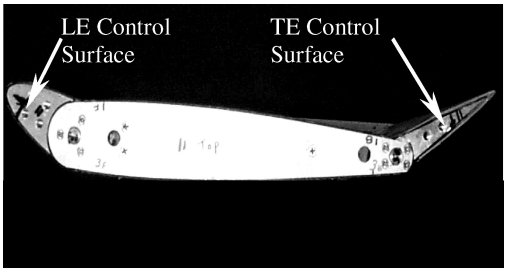

b)

Fig. 3 Dual-control surface airfoil showing a) top view with transparent skin revealing actuators, encoders, and connections and b) section view with the control surfaces deflected from their initial positions.

compact state-space form:

$$\dot{\boldsymbol{x}} = f_\mu(\boldsymbol{x}) + \boldsymbol{g}_1(\boldsymbol{x})U^2\beta + \boldsymbol{g}_2(\boldsymbol{x})U^2\gamma \tag{4}$$

where

$$\boldsymbol{x} = \{h \quad \alpha \quad \dot{h} \quad \dot{\alpha}\}^T = \{x_1 \quad x_2 \quad x_3 \quad x_4\}^T \tag{5}$$

$$f_\mu = \begin{Bmatrix} x_3 \\ x_4 \\ -k_1x_1 - \left[k_2U^2 + p(x_2)\right]x_2 - c_1x_3 - c_2x_4 \\ -k_3x_1 - \left[k_4U^2 + q(x_2)\right]x_2 - c_3x_3 - c_4x_4 \end{Bmatrix} \tag{6}$$

$$\boldsymbol{g}_1 = \{0 \quad 0 \quad g_{13} \quad g_{14}\}^T, \qquad \boldsymbol{g}_2 = \{0 \quad 0 \quad g_{23} \quad g_{24}\}^T \tag{7}$$

and the system variables are as follows:

$$D = m_T I_a - (m_W x_\alpha b)^2, \qquad p(x_2) = -(m_W x_\alpha b)k_\alpha/D$$

$$q(x_2) = m_T k_\alpha/D, \qquad k_1 = I_\alpha k_h/D$$

$$k_2 = \left(I_\alpha \rho bsC_{l_\alpha} + m_W x_\alpha \rho sb^3 C_{m_\alpha}\right)/D, \qquad k_3 = -m_W x_\alpha b k_h/D$$

$$k_4 = -\left(m_W x_\alpha \rho sb^2 C_{l_\alpha} + m_T \rho sb^2 C_{m_{\alpha-\text{eff}}}\right)/D$$

$$c_1 = \left[I_\alpha\left(c_h + \rho U sbC_{l_\alpha}\right) + m_W x_\alpha \rho U sb^3 C_{m_{\alpha-\text{eff}}}\right]/D$$

$$c_2 = \left[I_\alpha \rho U sb^2 C_{l_\alpha}(0.5 - a) - m_W x_\alpha bc_\alpha + m_W x_\alpha \rho U sb^4 C_{m_{\alpha-\text{eff}}}(0.5 - a)\right]/D$$

$$c_3 = \left[-m_W x_\alpha b\left(c_h + \rho U bsC_{l_\alpha}\right) - m_T \rho U sb^2 C_{m_{\alpha-\text{eff}}}\right]/D$$

$$c_4 = m_T\left\{\left[c_\alpha - \rho U sb^3 C_{m_{\alpha-\text{eff}}}(0.5 - a)\right] - m_W x_\alpha \rho U sb^3 C_{l_\alpha}(0.5 - a)\right\}/D$$

The g_{ij} variables are defined as

$$g_{13} = \left[-I_\alpha \rho bsC_{l_\beta} - m_W x_\alpha b^3 s\rho C_{m_{\beta-\text{eff}}}\right]/D$$

$$g_{14} = \left[m_W x_\alpha b^2 \rho sC_{l_\beta} + m_T \rho sb^2 C_{m_{\beta-\text{eff}}}\right]/D$$

$$g_{23} = \left[-I_\alpha \rho bsC_{l_\gamma} - m_W x_\alpha b^3 s\rho C_{m_{\gamma-\text{eff}}}\right]/D$$

$$g_{24} = \left[m_W x_\alpha b^2 \rho sC_{l_\gamma} + m_T \rho sb^2 C_{m_{\gamma-\text{eff}}}\right]/D \tag{8}$$

Two output functions are considered because two control surfaces are available. For the pitch and plunge output, the following output function is defined:

$$y(\boldsymbol{x}) = \begin{Bmatrix} y_1(\boldsymbol{x}) \\ y_2(\boldsymbol{x}) \end{Bmatrix} = \begin{Bmatrix} x_1 \\ x_2 \end{Bmatrix} = \begin{Bmatrix} h \\ \alpha \end{Bmatrix} \tag{9}$$

The relative degree, which is the number of differentiations of the output function, $y(\boldsymbol{x})$, required to obtain the input explicitly, may be found by use of approaches described in Ref. 8 and 12 (with essential results shown here), using Lie derivatives, where $L_f y(\boldsymbol{x})$ is a Lie derivative (see Ref. 17) of y in the direction of f,

$$L_f y(\boldsymbol{x}) = \sum_i \frac{\partial y}{\partial x_i} f_i \tag{10}$$

For both output functions, the relative degree is 2. In defining a linearizing transformation, a control influence matrix is required and defined as

$$A(\boldsymbol{x}) = \begin{bmatrix} L_{g_1}L_f y_1(\boldsymbol{x}) & L_{g_2}L_f y_1(\boldsymbol{x}) \\ L_{g_1}L_f y_2(\boldsymbol{x}) & L_{g_2}L_f y_2(\boldsymbol{x}) \end{bmatrix} = \begin{bmatrix} g_{13} & g_{23} \\ g_{14} & g_{24} \end{bmatrix} \tag{11}$$

For the system to be completely feedback linearizable, the control influence matrix must not be singular. The determinant of $A(x)$ is

$$|A(\boldsymbol{x})| = \rho^2 s^2 b^3\left(m_W^2 x_\alpha^2 b^2 - I_\alpha m_T\right)\left(C_{m_{\beta-\text{eff}}}C_{l_\gamma} - C_{l_\beta}C_{m_{\gamma-\text{eff}}}\right)(1/D) \tag{12}$$

This suggests that singularities will occur if $m_W^2 x_\alpha^2 b^2 = I_\alpha m_T$ or $C_{m_{\beta-\text{eff}}}C_{l_\gamma} = C_{l_\beta}C_{m_{\gamma-\text{eff}}}$, in which case the system will no longer be completely feedback linearizable. Note that for a leading-edge–trailing-edge control surface configuration $A(\boldsymbol{x})$ will never be singular. The first parenthesis in Eq. (12) will not be zero for any logical configuration of the system, and the two terms of the second parenthesis always have opposite signs; thus, $C_{m_{\beta-\text{eff}}}C_{l_\gamma} - C_{l_\beta}C_{m_{\gamma-\text{eff}}}$

will never be zero. For a nonsingular $A(\boldsymbol{x})$, the system is transformed using the following:

$$\phi_1 = y_1 = x_1 = h, \qquad \phi_2 = L_f y_1 = x_3 = \dot{h}$$
$$\phi_3 = y_2 = x_2 = \alpha, \qquad \phi_4 = L_f y_2 = x_4 = \dot{\alpha} \tag{13}$$

Therefore, transforming the equations of motion yields

$$\dot{\phi}_1 = \phi_2, \qquad \dot{\phi}_2 = L_f^2 y_1 + L_{g_1} L_f y_1 U^2 \beta + L_{g_2} L_f y_1 U^2 \gamma$$
$$\dot{\phi}_3 = \phi_4, \qquad \dot{\phi}_4 = L_f^2 y_2 + L_{g_1} L_f y_2 U^2 \beta + L_{g_2} L_f y_2 U^2 \gamma \tag{14}$$

From Eq. (14), one has

$$L_f^2 y_1(\boldsymbol{x}) = -k_1\phi_1 - \left[k_2 U^2 + p(\phi_3)\right]\phi_3 - c_1\phi_2 - c_2\phi_4$$
$$L_f^2 y_2(\boldsymbol{x}) = -k_3\phi_1 - \left[k_4 U^2 + q(\phi_3)\right]\phi_3 - c_3\phi_2 - c_4\phi_4 \tag{15}$$

The parameters containing the nonlinear stiffness terms in Eq. (15) are defined as

$$p(\phi_3) = (-m_W x_\alpha b/D)k_\alpha(\phi_3), \qquad q(\phi_3) = (m_T/D)k_\alpha(\phi_3)$$
$$k_\alpha(\phi_3) = k_{\alpha 0} + k_{\alpha 1}\phi_3 + \cdots + k_{\alpha N}\phi_3^N \tag{16}$$

where $k_\alpha(\phi_3)$ is the nonlinear pitch stiffness assumed to behave as an Nth-order polynomial. The stiffness terms are defined by θ_i and the terms in Eq. (15) containing $p(\phi_3)$ and $q(\phi_3)$ are written as

$$p(\phi_3)\phi_3 = \frac{-m_W x_\alpha b}{D}\left(\theta_1 + \theta_2\phi_3 + \cdots + \theta_N\phi_3^{N-1}\right)\phi_3$$
$$= \frac{-m_W x_\alpha b}{D}\sum_{i=1}^{N}\theta_i\phi_3^i \tag{17a}$$

$$q(\phi_3)\phi_3 = \frac{m_T}{D}\left(\theta_1 + \theta_2\phi_3 + \cdots + \theta_N\phi_3^{N-1}\right)\phi_3$$
$$= \frac{m_T}{D}\sum_{i=1}^{N}\theta_i\phi_3^i \tag{17b}$$

Two row matrices, $\boldsymbol{R}_1(\phi_3)$ and $\boldsymbol{R}_2(\phi_3)$, are defined. $R_{1i}(\phi_3)$ and $R_{2i}(\phi_3)$ are the ith terms of the respective row matrices and are written as

$$R_{1i}(\phi_3) = (-m_W x_\alpha b/D)\phi_3^i, \qquad R_{2i}(\phi_3) = (m_T/D)\phi_3^i \tag{18}$$

Now let the linear part of Eq. (15) be defined by the following functions:

$$F_1(\phi) = -k_1\phi_1 - k_2 U^2\phi_3 - c_1\phi_2 - c_2\phi_4$$
$$F_2(\phi) = -k_3\phi_1 - k_4 U^2\phi_3 - c_3\phi_2 - c_4\phi_4 \tag{19}$$

As a consequence, $\dot{\phi}_2$ and $\dot{\phi}_4$ from Eq. (15) are written as

$$\dot{\phi}_2 = F_1(\phi) - \sum_{i=1}^{N}\theta_i R_{1i}(\phi_3) + g_{13}U^2\beta + g_{23}U^2\gamma$$
$$\dot{\phi}_4 = F_2(\phi) - \sum_{i=1}^{N}\theta_i R_{2i}(\phi_3) + g_{14}U^2\beta + g_{24}U^2\gamma \tag{20}$$

If one defines the terms of the stiffness polynomial as a column matrix, $\boldsymbol{\Theta} = [\theta_1 \ \cdots \ \theta_N]^T$, then Eq. (20) may be written more compactly as

$$\begin{Bmatrix}\dot{\phi}_2\\ \dot{\phi}_4\end{Bmatrix} = \boldsymbol{F}(\phi) - \boldsymbol{R}(\phi_3)\boldsymbol{\Theta} + AU^2\boldsymbol{\beta} \tag{21}$$

where $\boldsymbol{R}(\phi_3) = [\boldsymbol{R}_1(\phi_3) \ \ \boldsymbol{R}_2(\phi_3)]^T$ and $\boldsymbol{\beta} = [\beta \ \ \gamma]^T$. If an equivalent control input $\boldsymbol{\nu}$ is defined as

$$\boldsymbol{\nu}(\phi) = \boldsymbol{F}(\phi) - \boldsymbol{R}(\phi_3)\boldsymbol{\Theta} + AU^2\boldsymbol{\beta} \tag{22}$$

then the following control law is obtained:

$$\boldsymbol{\beta} = -A^{-1}U^{-2}[\boldsymbol{F}(\phi) - \boldsymbol{R}(\phi_3)\boldsymbol{\Theta} - \boldsymbol{\nu}(\phi)] \tag{23}$$

Thus, the linearized system is

$$\begin{Bmatrix}\dot{\phi}_1\\ \dot{\phi}_3\\ \dot{\phi}_2\\ \dot{\phi}_4\end{Bmatrix} = \begin{Bmatrix}\phi_2\\ \phi_4\\ \boldsymbol{\nu}(\phi)\end{Bmatrix} \tag{24}$$

Adaptive Control

Adaptive control methods will augment the feedback linearized system to account for the inexact cancellation of the nonlinear parameters caused by modeling uncertainties. When one considers the Benchmark Active Control Technology (BACT)[18] model as a benchmark to validate our efforts, there are important restrictions, such as low wind-tunnel speeds and linear aerodynamics, where our model is valid. A derivation of a model reference based adaptive controller extended to a wing section with two control surfaces is presented, which parallels the efforts presented by Ko et al.[12] With feedback linearization, the formulation is now cast so that uncertainties may be introduced for the nonlinear stiffness terms, and the adaptive control law may be obtained. An estimation parameter $\hat{\boldsymbol{\Theta}}$ is now introduced to the control law in Eq. (23) for the stiffness terms; thus, the following is obtained:

$$\boldsymbol{\beta} = -A^{-1}U^{-2}[\boldsymbol{F}(\phi) - \boldsymbol{R}(\phi_3)\hat{\boldsymbol{\Theta}} - \boldsymbol{\nu}(\phi)] \tag{25}$$

The control is now substituted into Eq. (21) to obtain the linearized equation

$$\begin{Bmatrix}\dot{\phi}_2\\ \dot{\phi}_4\end{Bmatrix} = -\boldsymbol{R}(\phi_3)\{\boldsymbol{\Theta} - \hat{\boldsymbol{\Theta}}\} + \boldsymbol{\nu}(\phi) \tag{26}$$

Define $\tilde{\boldsymbol{\Theta}} \equiv \boldsymbol{\Theta} - \hat{\boldsymbol{\Theta}}$, the error between the modeled and estimated parameters, and rewrite Eq. (26),

$$\begin{Bmatrix}\dot{\phi}_2\\ \dot{\phi}_4\end{Bmatrix} = -\boldsymbol{R}(\phi_3)\tilde{\boldsymbol{\Theta}} + \boldsymbol{\nu}(\phi) \tag{27}$$

The linearized system may now be obtained by combining Eq. (27) with $\dot{\phi}_1$ and $\dot{\phi}_3$ as defined in Eq. (14),

$$\begin{Bmatrix}\dot{\phi}_1\\ \dot{\phi}_3\\ \dot{\phi}_2\\ \dot{\phi}_4\end{Bmatrix} = \begin{Bmatrix}\phi_2\\ \phi_4\\ -\boldsymbol{R}_1(\phi_3)\tilde{\boldsymbol{\Theta}}\\ -\boldsymbol{R}_2(\phi_3)\tilde{\boldsymbol{\Theta}}\end{Bmatrix} + \begin{Bmatrix}0_{2\times 1}\\ \boldsymbol{\nu}(\phi)\end{Bmatrix} \tag{28}$$

Let the equivalent control input $\boldsymbol{\nu}(\phi)$ be defined as

$$\boldsymbol{\nu}(\phi) = \begin{Bmatrix}a_1\phi_2 + a_2\phi_1\\ a_3\phi_4 + a_4\phi_3\end{Bmatrix} \tag{29}$$

where $a_1, \ldots, a_4$ can be determined using any standard linear control method. The linearized system defined in Eq. (28) may now be rewritten as

$$\begin{Bmatrix}\dot{\phi}_1\\ \dot{\phi}_3\\ \dot{\phi}_2\\ \dot{\phi}_4\end{Bmatrix} = \begin{bmatrix}0 & 0 & 1 & 0\\ 0 & 0 & 0 & 1\\ a_2 & 0 & a_1 & 0\\ 0 & a_4 & 0 & a_3\end{bmatrix}\begin{Bmatrix}\phi_1\\ \phi_3\\ \phi_2\\ \phi_4\end{Bmatrix} + \begin{Bmatrix}0\\ 0\\ -\boldsymbol{R}_1(\phi_3)\tilde{\boldsymbol{\Theta}}\\ -\boldsymbol{R}_2(\phi_3)\tilde{\boldsymbol{\Theta}}\end{Bmatrix} \tag{30a}$$

or more compactly as

$$\dot{\phi} = \tilde{A}\phi + \begin{Bmatrix} \mathbf{0}_{2\times 1} \\ -\boldsymbol{R}(\phi_3)\tilde{\Theta} \end{Bmatrix} \tag{30b}$$

The following Lyapunov function may now be used to determine the update law:

$$V = \tfrac{1}{2}\phi^T\phi + \tfrac{1}{2}\tilde{\Theta}^T\tilde{\Theta} \tag{31}$$

Differentiating with respect to time gives

$$\begin{aligned} \dot{V} &= \phi^T\dot{\phi} + \tilde{\Theta}^T\dot{\tilde{\Theta}} \\ &= \phi^T\left\{\tilde{A}\phi + \begin{Bmatrix} \mathbf{0}_{2\times 1} \\ -\boldsymbol{R}(\phi_3)\tilde{\Theta} \end{Bmatrix}\right\} + \tilde{\Theta}^T\dot{\tilde{\Theta}} \\ &= \phi^T\tilde{A}\phi - \phi_2\tilde{\Theta}^T\boldsymbol{R}_1^T(\phi_3) - \phi_4\tilde{\Theta}^T\boldsymbol{R}_2^T(\phi_3) + \tilde{\Theta}^T\dot{\tilde{\Theta}} \end{aligned} \tag{32}$$

From the last three terms in Eq. (32), the update law is found by first letting

$$-\phi_2\tilde{\Theta}^T\boldsymbol{R}_1^T(\phi_3) - \phi_4\tilde{\Theta}^T\boldsymbol{R}_2^T(\phi_3) + \tilde{\Theta}^T\dot{\tilde{\Theta}} = 0$$

$$\tilde{\Theta}^T\left[-\phi_2\boldsymbol{R}_1^T(\phi_3) - \phi_4\boldsymbol{R}_2^T(\phi_3) + \dot{\tilde{\Theta}}\right] = 0 \tag{33}$$

Because $\tilde{\Theta}^T \neq 0$, the update law for the estimates of the stiffness coefficients is found by recognizing that the bracketed term must be zero. Thus, the bracketed term is solved for $\dot{\tilde{\Theta}}$,

$$\dot{\tilde{\Theta}} = \left[\phi_2\boldsymbol{R}_1^T(\phi_3) + \phi_4\boldsymbol{R}_2^T(\phi_3)\right] \tag{34a}$$

or, taking the time derivative of $\tilde{\Theta} = \Theta - \hat{\Theta}$ and recognizing that $\dot{\Theta} = 0$, one gets

$$\dot{\tilde{\Theta}} = -\left[\phi_2\boldsymbol{R}_1^T(\phi_3) + \phi_4\boldsymbol{R}_2^T(\phi_3)\right] \tag{34b}$$

Because $\tilde{A}$ is chosen to be a negative-definite matrix, the first term of $\dot{V} < 0$. When the update law defined by Eq. (34b) is used, $\dot{V} \leq 0$ is guaranteed, thus guaranteeing stability of the system. The preceding update law does not necessarily guarantee convergence of the parameters; however, parameter convergence is not a necessary condition for stability of the linearized system in Eq. (30a). The invariant manifold theorem of LaSalle and Lefschetz[19] guarantees stability of the system.

The equivalent control vector $\boldsymbol{\nu}$ may be determined using Eq. (24), by using an LQR approach. The following index was minimized:

$$J = \int_0^\infty [\phi^T Q\phi + \boldsymbol{\nu}^T R\boldsymbol{\nu}]\,\mathrm{d}t \tag{35}$$

Various control input selections $\boldsymbol{\nu}$ are evaluated for performance and representative results are shown. Typically, large penalties on $\boldsymbol{\nu}$, that is, large R values, lead to small gains on $\boldsymbol{\nu}$ and less saturation of the control surfaces, but controlled response is slower, whereas small penalties on $\boldsymbol{\nu}$ lead to larger control gains and more saturation of the control surfaces, but the response is quicker.

Results

From static measurements on the nonlinear pitch cam, a polynomial model of the stiffness is found,

$$k(\alpha) = 12.77 + 53.47\alpha + 1003\alpha^2 \tag{36}$$

which is compared with measurements as shown in Fig. 4. The linearized form of the stiffness leads to a predicted linear flutter velocity of approximately 11.4 m/s. A phase portrait is provided in Fig. 5, which shows agreement between predicted and measured LCO motion of the wing section. In wind-tunnel experiments, LCOs first appear at ~13 m/s. From predictions, LCOs first appear at 10.6 m/s. The difference in the LCO onset velocities between predicted and measured values may be attributed to modeling uncertainties, as well as Coulomb friction (negligible at high-speed motion, dominant at low-speed motion), which may delay the onset of LCOs on the apparatus. For the physical parameters provided in Table 1, the damped natural frequencies of the system (linearized) are presented in Table 2, at zero freestream velocity. The independent frequencies are those considered when one degree of freedom is locked down, while the other is left free. The first predictions of the coupled system are made by considering the eigenvalues of the linearized system, with the second set of predictions derived from a fast Fourier transform (FFT) analysis on simulated data. Note that consistent results are obtained between predictions and measurements.

Control designs are evaluated through simulations and wind-tunnel experiments. To emphasize the importance for multiple control surfaces, that is, an additional control surface at the leading edge, results are presented for a single, trailing-edge control surface for comparison. Figures 6 and 7 show a closed-loop controlled

Table 2 Predicted and measured modal frequencies at $U = 0$ m/s

Frequency	Predicted, Hz	Predicted,* Hz	Measured, Hz
		Uncoupled	
$f_{pi-\text{damped}}$	1.509	1.772	1.465
$f_{pl-\text{damped}}$	2.146	2.151	2.051
		Coupled	
$f_{pi-\text{damped}}$	1.429	1.565	1.768
$f_{pl-\text{damped}}$	2.460	2.739	2.636

*FFT on simulated data.

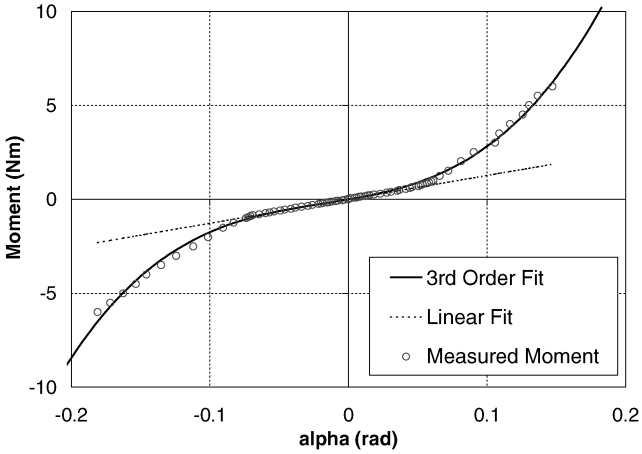

Fig. 4 Static measurements and polynomial fit for the structural response in the pitch mode.

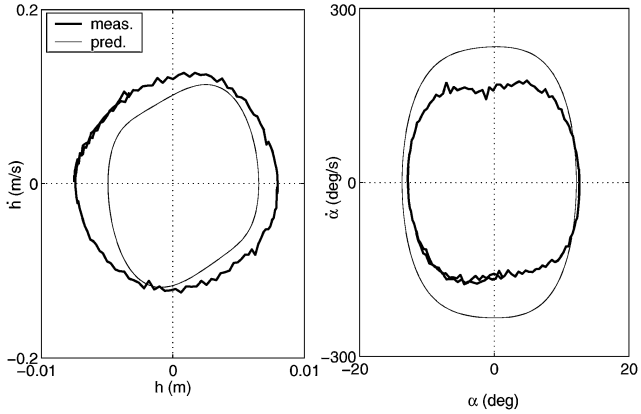

Fig. 5 Phase portrait of predicted and measured LCOs at $U = 13.01$ m/s.

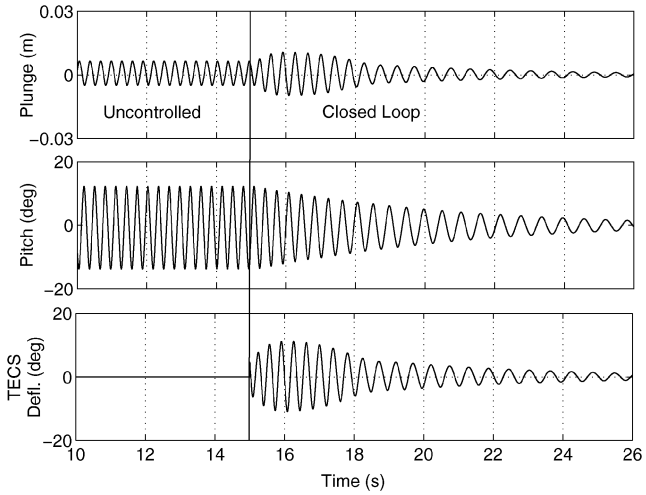

Fig. 6 Predicted response with trailing-edge control surface actuation at $U = 13.15$ m/s.

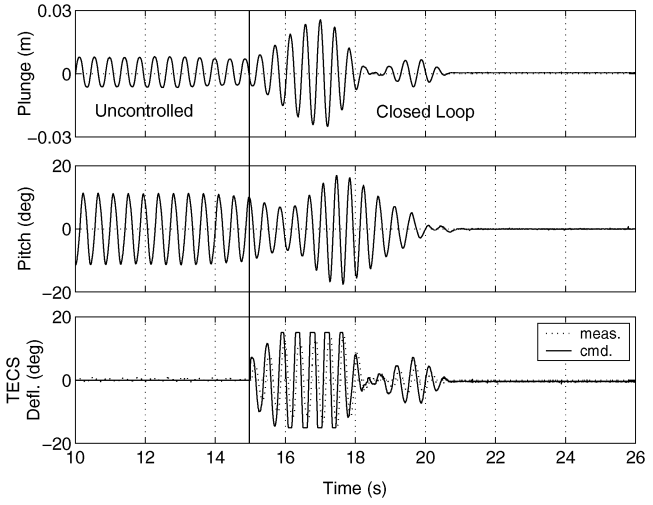

Fig. 7 Measured response with trailing-edge control surface actuation at $U = 13.15$ m/s.

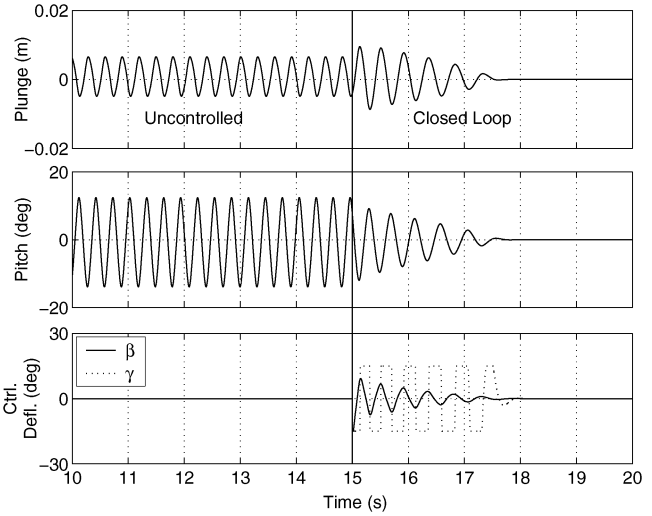

Fig. 8 Predicted response with leading-edge, γ, and trailing-edge, β, edge control surface actuation at $U = 13.28$ m/s.

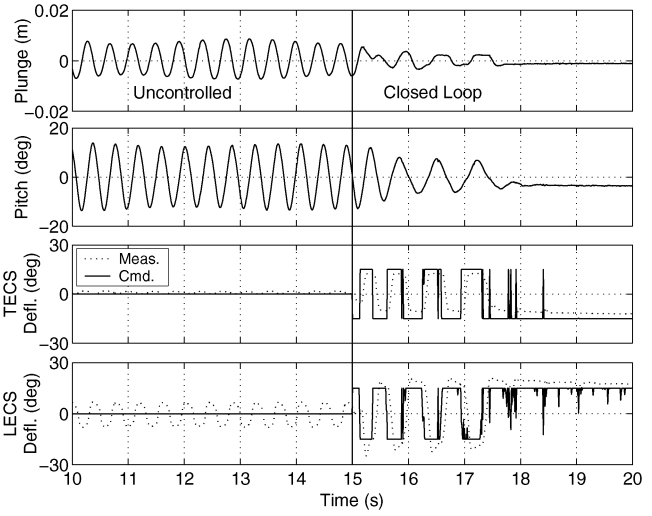

Fig. 9 Measured response with leading- and trailing-edge control surface actuation at $U = 13.28$ m/s.

response case using only the trailing-edge control surface. In this case, adaptive control is used with partial-feedback linearization and a control parameter chosen as $\nu = -0.4472\dot{\alpha} - 0.1\alpha$ because the control deflection limits are achieved with minimal saturation. The controller appears to work well both in theory and in practice; however, in wind-tunnel experiments for the new wing section, the single-surface controller only works for a limited range of freestream velocities. Above 13.4 m/s, control authority was lost and may be attributed to inevitable uncertainties in the structural stiffness or aerodynamic model, sensitivity to physical parameter uncertainty, and control parameter selection. Similar limitations are discussed in Ref. 12. One difficulty in determining the control parameter is that the transformed system is being used to minimize the performance index [Eq. (35)] and this control parameter is the equivalent control parameter that is also being solved for, rather than the actual control deflections. In theory, using a single, trailing-edge control surface may work independent of parameter and control selection, but the single controller is limited in practice. Kurdila et al.[15] have previously shown that using a single actuator provides no guarantee in suppressing LCOs.

Next, we examine the configuration with two control surfaces. The adaptive controller with full feedback linearization is tested for a range of freestream velocities by slowly increasing the wind-tunnel velocity and testing the control law effectiveness. Figures 8 and 9 show predicted and measured results using two control surfaces for small R values (low penalties on the control) and with the control surface deflections limited to 15 deg. The predictions show a quick response in the suppression of LCOs, with stabilization occurring within approximately 2–3 s, and agree with the experimental results. The spikes in the command signals, noted after the wing section has been stabilized, may be attributed to electrical noise, or commands issued due to small displacements caused by gusts (and, thus, fed back to the control law). At freestream velocities below 17 m/s, the control surfaces respond to the commands issued.

It is expected that the wing section would reach a equilibrium position at zero in both pitch and plunge. However, the wing section stabilizes at a nonzero equilibrium, with the two control surfaces deflected in opposite directions. A nonzero plunge position may be attributed to unmodeled Coulomb friction, stopping the wing section motion before it reaches zero, thus, feeding back a nonzero position to the control law. Also, the aerodynamic loading may prevent the leading-edge control surface from properly responding when the control surface is at its deflection limit. As a consequence, the trailing-edge control surface will deflect to eliminate the aerodynamic moment produced by the leading-edge control surface, which will influence the angle of attack of the wing section. As the freestream velocity approaches 17 m/s, the controller effectiveness deteriorates, and beyond 17 m/s, the controller is ineffective at suppressing LCOs. At higher velocities, the aerodynamic loading exceeds the load limits on the leading-edge control surface actuators, adversely affecting response to commands. With the

leading-edge control surface rendered ineffective, the trailing-edge control surface alone will not stabilize the wing section. Furthermore, unmodeled nonlinear aerodynamic effects, as well as unsteady effects, become an issue at higher freestream velocities. Although leading-edge control surface motion is observed at low freestream velocities, no adverse effects are observed during control actuation. Yet, control surface dynamics for the actuators currently used will be an issue at higher velocities.

Conclusions

A control approach based on adaptive feedback linearization with a model-reference-based control law is developed for implementation in a nonlinear aeroelastic system, namely, a wing with nonlinear structural responses and with control actuation provided by both leading- and trailing-edge control surfaces. Predictions of both free responses and closed-loop controlled responses of the nonlinear system compare well with experiments. Comparisons with predicted and measured results for a wing section with only the trailing-edge control surface show the advantage of control strategies with multiple control surfaces. Predicted responses using the presented control law show good performance; yet, in practice, the effectiveness is limited by hardware design at higher freestream velocities because of larger aerodynamic loads acting on the control surfaces, an increased sensitivity to nonlinear and unsteady aerodynamic effects, and control surface dynamics.

References

[1]Rule, J. A., Richard, R. E., and Clark, R. L., "Design of an Aeroelastic Delta Wing Model for Active Flutter Control," *Journal of Guidance, Control, and Dynamics*, Vol. 24, No. 5, 2001, pp. 919–924.

[2]Wazak, M., and Srinathkumar, S., "Design and Experimental Validation of a Flutter Suppression Controller for the Active Flexible Wing," NASA TM 4381, Office of Management, Scientific and Technical Information Program, Washington, DC, 1992.

[3]Mukhopadhyay, V., "Flutter Suppression Digital Control Law Design and Testing for the AFW Wind Tunnel Model," NASA TM 107652, Langley Research Center, Hampton, VA, 1992.

[4]Vipperman, J. S., Barker, J. M., Clark, R. L., and Balas, J. S., "Comparison of μ- and H_2-Synthesis Controllers on an Experimental Typical Section," *Journal of Guidance, Control, and Dynamics*, Vol. 22, No. 2, 1999, pp. 278–285.

[5]Denegri, C. M., Jr., and Johnson, M. R., "Limit-Cycle Oscillation Prediction Using Artificial Neural Networks," *Journal of Guidance, Control, and Dynamics*, Vol. 24, No. 5, 2001, pp. 887–895.

[6]Denegri, C. M., Jr., and Cutchins, M. A., "Evaluation of Classical Flutter Analysis for the Prediction of Limit Cycle Oscillations," AIAA Paper 97-1021, April 1997.

[7]Block, J. J., and Strganac, T. W., "Applied Active Control for a Nonlinear Aeroelastic Structure," *Journal of Guidance, Control, and Dynamics*, Vol. 21, No. 6, 1998, pp. 838–845.

[8]Ko, J., Kurdila, A. J., and Strganac, T. W., "Nonlinear Control of a Prototypical Wing Section with Torsional Nonlinearity," *Journal of Guidance, Control, and Dynamics*, Vol. 20, No. 6, 1997, pp. 1181–1189.

[9]Ko, J., Strganac, T. W., and Kurdila, A. J., "Stability and Control of a Structurally Nonlinear Aeroelastic System," *Journal of Guidance, Control, and Dynamics*, Vol. 21, No. 5, 1998, pp. 718–725.

[10]Xing, W., and Singh, S. N., "Adaptive Output Feedback Control of a Nonlinear Aeroelastic Structure," *Journal of Guidance, Control, and Dynamics*, Vol. 23, No. 6, 2000, pp. 1109–1116.

[11]Zhang, R., and Singh, S. N., "Adaptive Output Feedback Control of an Aeroelastic System with Unstructured Uncertainties," *Journal of Guidance, Control, and Dynamics*, Vol. 24, No. 3, 2001, pp. 503–509.

[12]Ko, J., Strganac, T. W., and Kurdila, A. J., "Adaptive Feedback Linearization for the Control of a Typical Wing Section With Structural Nonlinearity," *Nonlinear Dynamics*, Vol. 18, No. 3, 1999, pp. 289–301.

[13]Strganac, T. W., Ko, J., and Thompson, D. E., "Identification and Control of Limit-Cycle Oscillations in Aeroelastic Systems," *Journal of Guidance, Control, and Dynamics*, Vol. 23, No. 6, 2000, pp. 1127–1133.

[14]Strganac, T. W., Ko, J., Thompson, D. E., and Kurdila, A. J., "Investigations of Limit Cycle Oscillations in Aeroelastic Systems," NASA CP-1999-209136, June 1999.

[15]Kurdila, A., Strganac, T., Junkins, J., Ko, J., and Akella, M., "Nonlinear Control Methods for High-Energy Limit-Cycle Oscillations," *Journal of Guidance, Control and Dynamics*, Vol. 24, No. 1, 2001, pp. 185–192.

[16]Thompson, D., "Nonlinear Analysis of Store-Induced Limit Cycle Oscillations," M.S. Thesis, Dept. of Aerospace Engineering, Texas A&M Univ., College Station, TX, Aug. 2001.

[17]Isidori, A., *Nonlinear Control Systems*, Springer-Verlag, New York, 1989, pp. 1–82.

[18]Mukhopadhyay, V., "Transonic Flutter Suppression Control Law Design, Analysis, and Wind Tunnel Results," NASA CP-1999-209136/PT-1, June 1999.

[19]La Salle, J., and Lefschetz, S., *Stability by Liapunov's Direct Method*, Academic Press, New York, 1961, pp. 37–73.